ChemComm

Accepted Manuscript

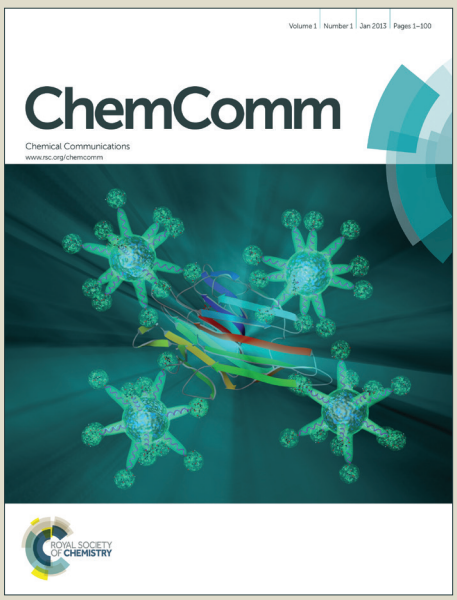

ROYAL SOCIETY OF CHEMISTRY

www.rsc.org/chemcomm

Cite this: DOI: 10.1039/c0xx00000x

www.rsc.org/xxxxxx

ARTICLE TYPE

Area Negative Thermal Expansion in a Beryllium Borate $LiBeBO_3$ with Edge Sharing Tetrahedra†

Wenjiao Yao,[a, d, ‡] Xingxing Jiang,[a, d, ‡] Rongjin Huang,*[b] Wei Li,[c] Chuanjun Huang,[b] Zheshuai Lin,*[a] Laifeng Li[b] and Chuangtian Chen[a]

Received (in XXX, XXX) Xth XXXXXXXXX 20XX, Accepted Xth XXXXXXXXX 20XX
DOI: 10.1039/b000000x

A very rare area negative thermal expansion phenomenon is observed in a newly discovered alkali beryllium borate $LiBeBO_3$, which features with $[BeBO_3]_\infty$ double layers intraconnected by edge-sharing BeO_4 tetrahedra. This unusual thermal behavior attributes to the combined vibration effects of the abnormal Be-O structures and Li^+ cations.

Most matters exhibit the normal thermal behavior that expand with heat and contract with cold. However, there are a very small number of materials, e.g., β-eucryptite, $NaZrPO_4$, and ZrW_2O_8, having a completely opposite property that contract in 1D, 2D or even 3D as the temperature increases.[1-4] These abnormal negative thermal expension (NTE) properties have attracted a great deals of attentions in laboratories and industries. Up to now, the NTE exploration mainly focuses on the compounds containing transition metals.[5] For borates, a big family with diverse structural features[6-8] and many optoelectronic applications,[9-11] the NTE investigation has not been systematically performed yet, and only the linear (1D) NTE phenomenon has been detected in several borates (e.g., $\alpha-RbB_3O_5$, LiB_3O_5, and BiB_3O_6).[12] In this work, we report a new beryllium borate $LiBeBO_3$ (LBBO) which exhibit a 2D *area* NTE behavior as first found in borates. This material is featured with $[BeBO_3]_\infty$ double layers intraconnected by edge-sharing BeO_4 tetrahedra. The detailed studies reveal that this unusual thermal phenomenon is resulted from the vibration effects of the abnormal Be-O structures combined with the Li^+ cations. Independently, Wang *et al.* have also reported the discovery of the LBBO crystal,[13] but they only focused on the crystallographic characterization.

LBBO was synthesized by solid state reaction and flux method in the R-BeO-B_2O_3 system (R is alkali oxide/halogenide). The compound crystallizes in the triclinic system with centrosymmetric space group *P-1*.[14] The framework of LBBO structure is featured by infinite two-dimensional $[Be_2B_2O_6]_\infty$ double-layers, with Li^+ cations located in the interlayers, as shown in Figure 1a. The double layer is formed by two interconnected $[BeBO_3]_\infty$ layers. Within the $[BeBO_3]_\infty$ layer, each B atom is coordinated by three O atoms to form a BO_3 triangle, and each Be atom is coordinated by four O atoms to form a distorted BeO_4 tetrahedron. The BeO_4 tetrahedra and BO_3 triangles are arrayed at interval by sharing corner oxygen atoms, as shown in Figure 1b. It is noteworthy that every two $[BeBO_3]_\infty$ layers are bonded together by the edge-sharing BeO_4 tetrahedra to form a $[Be_2O_2]$ configuration perpendicular to the layers; this interlayer connection pattern is first found in borates. The edge-sharing BeO_4 tetrahedra undulate the $[BeBO_3]_\infty$ layer and result in the shortest layer distance (2.655(4) Å) ever known in layered borates.

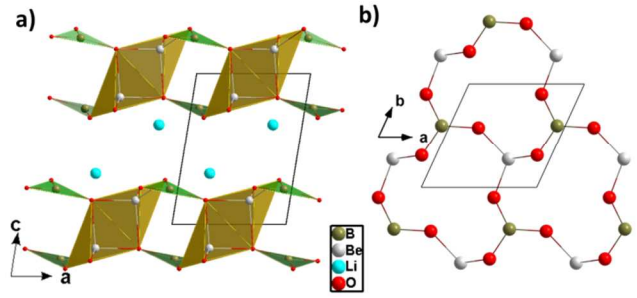

Figure. 1 Structure of LBBO. (a) Schematic diagram viewing along the *b*-axis. The green triangles and gold polyhedra represent $[BO_3]$ groups and $[BeO_4]$ tetrahedra, respectively. (b) The layered $[BeBO3]_\infty$ structure in the *ab* plane.

LBBO contains the $[Be_2O_6]$ structure with a Be_2O_2 parallelogram and two O–Be–O dendrites formed by two edge-sharing BeO_4 tetrahedra (see Figure S1). This atomic configuration is in confliction with the third Pauling's rule that suggests that the polyhedra would be more stable if they share vertices rather than edges or faces.[15] However, LBBO is very stable over a wide temperature range. The thermal differential scanning calorimetric analysis revealed that its structure remains unchanged until 1100 K, and the low and high temperature in situ XRD patterns are almost identical within the studied temperature range from 13 K to 848 K (Figure S2). The thermal stability is also confirmed by the first-principles calculations (see Supporting Information).

It is well known that a new structure feature often results in novel physical properties. Indeed, variable-temperature in situ powder X-ray diffraction revealed that LBBO exhibits an unusual area NTE phenomenon (the cell parameters are listed in Table S3). Abnormal thermal contracting for the *a* and *b* axis from 73 K to 193 K was observed, while the thermal expansion along the *c* axis is quite positive, as displayed in Figure 2a. The cell parameter data were then adopted to calculate the principal thermal expansivities across the above temperature range.[16] The

normalized components of the principal axes projected onto the crystallographic axes are given in Figure 2b (the relationship between principal axes *X*, *Y*, *Z* and crystallographic axes *a*, *b*, *c* given in Table S4). It is clear that the linear thermal expansion coefficients along *X* and *Y* axes are -3.31(13) MK^{-1} and -1.76(08) MK^{-1}, respectively, and the area thermal expansion coefficient in *X*-*Y* plane is -5.07(21) MK^{-1}. Even in the higher temperature range from 193 K to 273 K this compound still exhibits a linear NTE behaviour (along the *a*-axis, see Figure 2a).

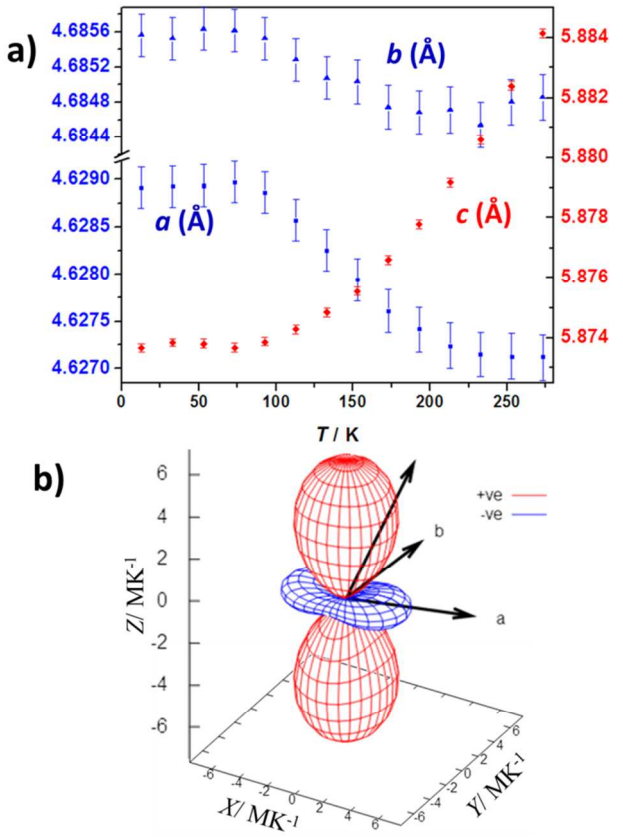

Figure 2. Thermal expansion behavior of the $LiBeBO_3$ (a) Variation of *a*, *b* and *c* axes verse temperature. (b) Normalized components of the principal axes verse temperature, where *X*, *Y*, and *Z* are -3.31(13) MK^{-1}, -1.76(08) MK^{-1}, and 7.58(76) MK^{-1}, determined by the PASCal program. [17]

To understand the mechanism for the NTE phenomenon in LBBO, we probe the atomic vibration modes in the IR and Raman spectra. It is well known that an atomic vibration mode would shift to lower wavenumbers, if the involved effective bond length is elongated and the chemical bonding becomes weaker as usually occurs at higher temperature.[17] However, the vibrational modes of 73 K and 193 K in Table S1 reveal that quite a few vibrational modes conversely shift to higher wavenumbers when the temperature increases. These atomic vibrations contribute to the lattice contraction as temperature increases. This conclusion is also confirmed by the first-principles analysis on the Grüneisen function[18] for respective vibration modes (see the Supporting Information). Further vibrational attribution analysis shows that these abnormal vibration modes mainly arise from the transitional vibration of Li^+ ions, the distorting vibration(stretching and rotation) of Be_2O_2 rings and BeO_4 tetrahedra, and the rigid vibration (swing and rotation) of BO_3 triangles, as indicated in Figure 3.

The detailed geometry comparison between 73 K and 193 K reveals that the angles inside the Be_2O_2 parallelogram (see Figure 3 and the crystallographic data given in the CIF files in the Supplementary Information) remain unchanged, while the ∠O2-Be-O3 angles increase about 0.2° and the ∠O1-Be-O3 angles decrease about 0.1°, which results in the rigid BO_3 triangles more tilted with respect to the $[BeBO_3]_\infty$ layers and makes the *ab* plane contracted. Meanwhile, with the increase of temperature the decrease of interaction between Li^+ cations and BO_3 groups further liberates the latter tilted toward the *c*-axis driven by the distortion of Be_2O_2 parallelogram. Therefore, the NTE effect in LBBO is mainly originated from the distortion of edge-sharing Be-O tetrahedra as well as the motion of alkali cations.

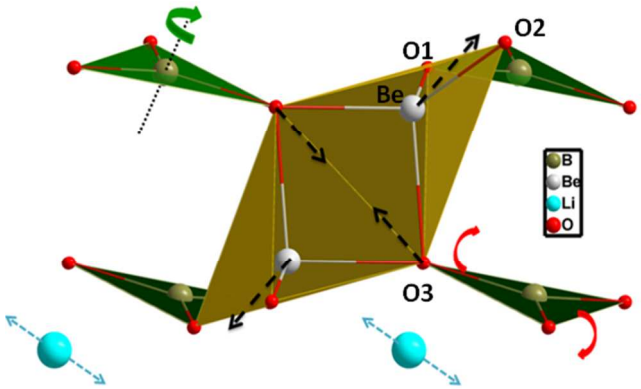

Figure 3. Schematic of the atomic vibration modes associated with NTE. The blue and black dotted lines indicate the transitional vibration of Li^+ atoms and the stretching of Be_2O_2 rings, respectively. The red and green curved arrows indicate the swing and rotation of BO_3 triangle respectively.

It should also be emphasized that LBBO has a high level of transparency in the ultraviolet (UV) spectral region and its cutoff wavelength extending to less than 200 nm (Figure 4), so it might be served as a UV and deep-UV optical material. Therefore, combined with the NTE property, LBBO might find important applications for temperature sensitive optical environments.[19] Examples include the thermal-expansion-adjustable component in the diffraction gratings and optical fibers, compensator in the precise UV optical instrument, and optical temperature sensor for ultrafine manufacture control and superconductor mechanism probing,[20] since the device sensitivity is proportional to the fractional change in optical path length with temperature.

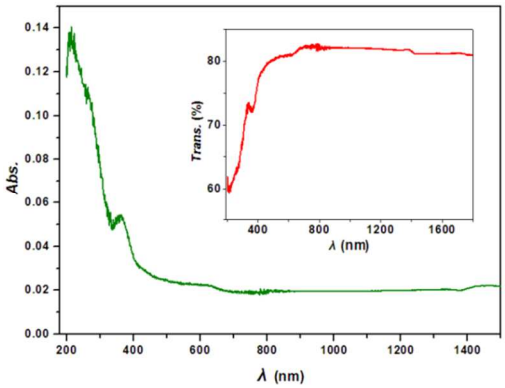

Figure 4. IR-Vis-UV diffuse-reflectance spectrum of $LiBeBO_3$

In conclusion, an area thermal contraction behavior in the temperatue range from 73 K and 193 K is identified in a new beryllium borate $LiBeBO_3$; this is the first borate that exhibits the NTE phenomenon in two-dimension. The unusual thermal behavior is intimately associated with a unique structural feature presented in $LiBeBO_3$, i.e., the double layers intra-connected by edge-sharing BeO_4 tetrahedra. Although the abnormal edge-sharing BeO_4 tetrahedron is counter to Pauling's Third rule, the structure of $LiBeBO_3$ is stable up to 1100 K. Moreover, $LiBeBO_3$ is transparent to deep UV spectral region. The extraordinary thermal and optical properties of $LiBeBO_3$ may find wide applications such as in photoelectronics, precision manufacture, and cryogenic engineering.

The authors acknowledge the financial support from the National Natural Science Foundation of China under Grant Nos 11474292, 11174297, 91022036, 61138004, and 51232004, the National Basic Research Project of China (Nos 2010CB630701 and 2011CB922204), and Special Foundation of the Director of Technical Institute of Physics and Chemistry, CAS.

Notes and references

[a] *Beijing Center for Crystal R&D, Key Lab of Functional Crystals and Laser Technology, Technical Institute of Physics and Chemistry (TIPC), Chinese Academy of Sciences (CAS), Beijing 100190, PR China. E-mail: zslin@mail.ipc.ac.cn*

[b] *Key Laboratory of Cryogenics, TIPC, CAS, Beijing, 100190, PR China. E-mail: huangrongjin@mail.ipc.ac.cn*

[c] *Department of Materials Science and Metallurgy, University of Cambridge, Cambridge CB3 0FS, UK*

[d] *University of Chinese Academy of Sciences, Beijing 100049, PR China*

† Electronic Supplementary Information (ESI) available: Exprimental details and additional data. See DOI: 10.1039/b000000x/

‡ These authors contributed equally.

1 (a) J. R. Salvador, F. Gu, T. Hogan, M. G. Kanatzidis, *Nature* 2003, **425**, 702. (b) A. Sleight, *Nature* 2003, **425**, 674.

2 T. A. Mary, J. S. O. Evans, T. Vogt, A. W. Sleight, *Science* 1996, **272**, 90−92.

3 X. Y. Song, Z. H. Sun, Q. Z. Huang, M. Rettenmayr, X. M. Liu, M. Seyring, G. N. Li, G. H. Rao, F. X. Yin, *Adv. Mater.* 2011, **23**, 4690-4694.

4 (a) S. A. Hodgson, J. Adamson, S. J. Hunt, M. J. Cliffe, A. B. Cairns, A. L. Thompson, M. G. Tucker, N. P. Funnell, A. L. Goodwin, *Chem. Comm.* 2014, **50**, 5264-5266. (b) A. B. Cairns, A. L. Thompson, M. G. Tucker, J. Haines, A. L. Goodwin, *J. Am. Chem. Soc.* 2012, **134**, 4454−4456.

5 C. Lind, *Materials* 2012, **5**, 1125-1154.

6 (a) S. C. Wang, N. Ye, W. Li, D. Zhao, *J. Am. Chem. Soc.* 2010, **132**, 8779−8786. (b) S. C. Wang, N. Ye, *J. Am. Chem. Soc.* 2011, **133**, 11458–11461. (c) H. P. Wu, S. L. Pan, K. R. Poeppelmeier, H. Y. Li, D. Z. Jia, Z. H. Chen, X. Y. Fan, Y. Yang, J. M. Rondinelli, H. S. Luo, *J. Am. Chem. Soc.* 2011, **133**, 7786.

7 (a) H. W. Huang, J. Y. Yao, Z. S. Lin, X. Y. Wang, R. He, W. J. Yao, N. X. Zhai, C. T. Chen, *Angew. Chem. Int. Ed.* 2011, **50**, 9141−9144. (b) H. W. Huang, J. Y. Yao, Z. S. Lin, X. Y. Wang, R. He, W. J. Yao, N. X. Zhai, C. T. Chen, *Chem. Mater.* 2011, **23**, 5457−5463. (c) H. W. Huang, L. J. Liu, S. F. Jin, W. J. Yao, Y. H. Zhang, C. T. Chen, *J. Am. Chem. Soc.* 2013, **135**, 18319−18322.

8 (a) W. J. Yao, R. He, X. Y. Wang, Z. S. Lin, C. T. Chen, *Adv. Opti. Mater.* 2014, DOI: 10.1002/adom.201300535. (b) W. J. Yao, X. X. Jiang, H. W. Huang, T. Xu, X. S. Wang, Z. S. Lin, C. T. Chen, *Inorg. Chem.* 2013, **52** (15), 8291-8293. (c) W. J. Yao, H. W. Huang, J. Y. Yao, T. Xu, X. X. Jiang, Z. S. Lin, C. T. Chen, *Inorg. Chem.* 2013, **52**, 6136− 6141.

9 C. T. Chen, T. Sasaki, in *Nonlinear Optical Borate Crystals-Principles and Applications*, Wiley-VCH, Weinheim, Germany, 2011.

10 (a) R. T. Mu, Q. Fu, L. Jin, L. Yu, G. Z. Fang, D. L. Tan, X. H. Bao, *Angew. Chem. Int. Ed.* 2012, **51**, 4856–4859. (b) Y. M. Xu, P. Richard, K. Nakayama, T. Kawahara, Y. Sekiba, T. Qian, M. Neupane, S. Souma, T. Sato, T. Takahashi, H. Q. Luo, H. H. Wen, G. F. Chen, N. L. Wang, Z. Wang, Z. Fang, X. Dai, H. Ding, *Nat. Commun.* 2011, **2**, 392. (c) Y. M. Xu, Y. B. Huang, X. Y. Cui, E. Razzoli, M. Radovic, M. Shi, G. F. Chen, P. Zheng, N. L. Wang, C. L. Zhang, P. C. Dai, J. P. Hu, Z. Wang, H. Ding, *Nat. Phys.* 2011, **7**, 198−202.

11 (a) D. Cyranoski, *Nature* 2009, **457**, 953−955. (b) R. D. Schaeffer, T. Hannon, *Laser Focus World* 2001, **37**, 115. (c) T. Sekikawa, A. Kosuge, T. Kanai, S. Watanabe, *Nature* 2004, **432**, 605−608.

12 (a) P. Becker, L. Bohaty, *Cryst. Res. Technol.* 2001, **36,** 1175-1180. (b) W. Lin, G. Q. Dai, Q. Z. Huang, A. Zhen, J. K. Liang, *J. Phys. D: Appl. Phys.* 1990, **23**, 1073−1075. (c) R. S. Bubnova, S. K. Filatov *Phys. Stat. Sol. b* 2008, **245**, 2469– 2476.

13 S. C. Wang, N. Ye, G. H. Zou, *Inorg. Chem.* 2014, 53, 2742-2748.

14 $LiBeBO_3$ single crystal was obtained with a molten flux based on LiF-BeO-B_2O_3-NaCl system. Crystal data for $LiBeBO_3$: Mr = 74.76, colorless platelet, 0.44 × 0.37 × 0.05 mm^3, triclinic, space group P-*1* (No. 2), a = 4.6214(9) Å, b = 4.6780(9) Å, c = 5.8704(12) Å, α = 68.24(3)°, β = 72.03(3)° γ = 61.08(3)°, V = 101.86(191) $Å^3$, Z = 2, ρ_{calcd} = 3.586 g cm^{-3}, graphite-monochromatized Mo Kα (λ = 0.71073 Å) on a Rigaku AFC10 diffractometer equipped with a Saturn CCD detector, $F(000)$ = 72, μ = 0.216 mm^{-1}, T = 143(2) K, 791 measured reflections in the range 3.7856° <2θ< 33.6876°, R(int) = 0.028; R_1 = 0.0283 and wR_2 = 0.0742 for all F_o^2. CSD-427287 (obtained at Jan 23, 2014).

15 (a) S. F. Jin, G. M. Cai, W. Y. Wang, M. He, S. C. Wang, X. L. Chen, *Angew. Chem. Int. Ed.* 2010, **49**, 4967–4970. (b) J. K. Burdett, Timothy J. McLarnan, *J. Am. Chem. Soc.* 1982, **104**, 5229-5230.

16 M. J. Cliffe, A. L. Goodwin, *J. Appl. Crystallog.* 2012, **45**, 1321–1329.

17 G. D. Barrera, J. A. Bruno, T. H. K. Barron, N. L. Allan, *J. Phys.: Condens. Matter*, 2005, **17**, R217−R252.

18 (a) W. Miller, C. W. Smith, D. S. Mackenzie, *J. Mater. Sci.* 2009, **44**, 5441. (b) John S. O. Evans, *Dalton Trans.* 1999, **17**, 3317-3326. (c) T. A. Mary, J. S. O. Evans, T. Vogt, A. W. Sleight, *Science* 1996, **272**, 90−92.

19 Y. Sun, C. Wang, Y. C. Wen, L. H. Chu, M. Nie, F. S. Liu, *J. Am. Ceram. Soc.* 2010, **93**, 650−653.

20 (a) I. E. Collings, M. G. Tucker, D. A. Keenb. A. L. Goodwin, *CrystEngCommun* 2014, **16**, 3498-3506. (b) K. Takenaka, *Sci. Technol. Adv. Mater.* 2012, **13**, 013001.